Chapter 10
Tunneling and Chaos

Since the early days of quantum mechanics, tunneling has been considered one of its symbols: the ability of quantum particles to penetrate through energy barriers is one of the most impressive applications of quantum theory. This phenomenon has numerous applications in atomic, molecular, and nuclear physics as well as in solid state physics. Almost a century has elapsed since its discovery, and the various aspects of tunneling have been studied, but only in the last decades has it become clear that despite its significantly quantum nature, tunneling is largely, if not entirely, determined by the structure of the classical phase space of the system. The transition of classical dynamics of integrability to chaos substantially modifies the tunneling process. The purpose of this chapter is to make a clear, at first glance, paradoxical statement: tunneling is absent in classical physics, but the structure of the classical phase space defines a purely quantum effect of the tunneling!

10.1 Tunneling in One-Dimensional Systems

As is well known, a quantum system can be completely described by its wave function $|\psi\rangle$, which represents a vector in Hilbert space in mathematical language. In particular, an isolated spinless particle can be represented by a wave function in the coordinate $\langle x|\psi\rangle$ or momentum $\langle p|\psi\rangle$ spaces. The same object in classical mechanics is described in the phase space by the coordinates x, p. The question is this: how can the classical time evolution described by Hamiltonian equations in terms of x, p be reflected in the quantum reality using a single vector $|\psi\rangle$ satisfying the Schrödinger equation? It seems natural to associate the classical particle with the quantum state $|\psi\rangle$, which is localized optimally in the vicinity of the particle's position in the classical phase space at any given time t. But quantum mechanics imposes a fundamental restriction on the limit of the localization, expressed by the

Y. Bolotin et al., *Chaos: Concepts, Control and Constructive Use*,
Understanding Complex Systems, DOI 10.1007/978-3-319-42496-5_10

uncertainty relation

$$\Delta x \cdot \Delta p \geq \hbar/2.$$

Similar relations also exist for other canonically conjugate variables. Hence, the maximum that we can hope for is to localize the particle in the domain of the finite dimensions $(\Delta x, \Delta p)$ around the position of the particle (x, p), with Δx, Δp being significantly less than the scales characterizing the classical trajectory. This should satisfy our desire to construct a quantum state that imitates the classical motion, provided that $|\psi\rangle$ follows the classical time evolution of x, p and $\Delta x, \Delta p$ remain small over time. Thus classical bodies are linked to the center of the gravity trajectory even if they have finite dimensions. The quantum state, which possesses such properties, at least in finite times, is called a wave packet (WP). Indeed, the WP is the tunneling object. Let us consider [1] a quantum system with Hamiltonian H, which performs one-dimensional finite motion. Its discrete spectrum E_i and stationary wave functions ψ_i are solutions of the equation

$$H\psi_i = E_i\psi_i.$$

The arbitrary WP $\Psi(t)$, initially localized in a domain R, can be represented as a superposition

$$\Psi(t=0) = \sum_i c_i\psi_i.$$

The property of the initial localization of the WP means that the integral of the square modulus of the wave function at time $t = 0$ is close to the normalization of the wave function

$$\int_R |\Psi(t=0)|^2 dx \simeq 1.$$

The temporal evolution of the WP is determined by the time-dependent stationary wave functions:

$$\Psi(x,t) = \sum_i c_i \exp\left(-iE_it/\hbar\right)\psi_i(x).$$

The probability $p_R(t)$ of remaining in the domain R at later moments t is a linear combination of periodic (trigonometric) functions with frequencies $|E_i - E_k|/\hbar$, where the indices i, k comply with all the components entering the WP. The typical time required for the WP to return to the initial state is of order the least common multiple of the inverse frequencies. Since in the general case, the frequencies are incommensurable, the WP will broaden with time to all available phase space.

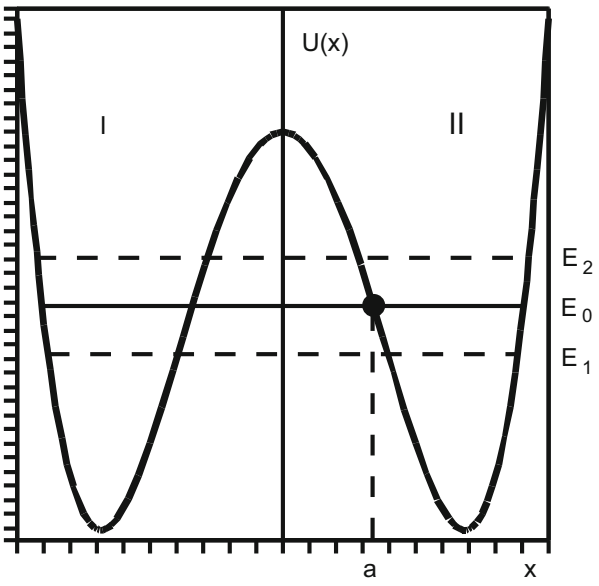

Fig. 10.1 Level splitting in symmetric one-dimensional potential double well

Packet components corresponding to the high frequencies (big$|E_i - E_k|$) will expand faster than the low-frequency components. The simplest WP is a packet consisting of only two components of the wave functions ψ_1 and ψ_2 and energies E_1 and E_2. This situation can adequately reflect the situation in the spectrum for which $|E_1 - E_2| \ll |E_i - E_1| \sim |E_i - E_2|$ for all other states ψ_i. In this case,

$$p_R(t) = p_R(0) - 4A\sin^2\left(|E_1 - E_2|\, t/\hbar\right), \tag{10.1}$$

where

$$A = c_1 c_2 \int_R \psi_1 \psi_2 dx$$

($c_{1,2}$ and $\psi_{1,2}$ are assumed to be real). This approximation can be used to describe the tunneling process in a one-dimensional symmetric double well, as shown in Fig. 10.1.

If the potential barrier between the wells *I* and *II* is impenetrable for a particle, then there are energy levels corresponding to the motion of particles in each well, and the same for the two wells. Consideration of the tunneling (the possibility of transition through the potential barrier) leads to the splitting of each of these levels into two close levels. The wave functions corresponding to these almost degenerate levels (due to the smallness of the interactions between the wells) describe the motion of a particle simultaneously in both wells. Let $\psi_0(x)$ be the

semiclassical wave function describing the motion with energy E_0 in an isolated well I, that is, exponentially damped on both sides of the boundaries of this well. When the tunneling is taken into account, the function $\psi_0(x)$ ceases to be a stationary wave function of the overall system, and the level E_0 splits into the levels E_1 and E_2. The correct wave functions corresponding to these levels are symmetric and antisymmetric combinations of the functions $\psi_0(x)$ and $\psi_0(-x)$:

$$\psi_1(x) = \frac{1}{\sqrt{2}}\left[\psi_0(x) + \psi_0(-x)\right],$$

$$\psi_2(x) = \frac{1}{\sqrt{2}}\left[\psi_0(x) - \psi_0(-x)\right]. \tag{10.2}$$

Using the semiclassical approximation for $\psi_0(x)$ [2], one can show that

$$\Delta E \equiv E_2 - E_1 = \frac{\omega\hbar}{\pi}\exp\left(-\frac{1}{\hbar}\int_{-a}^{a}|p|\,dx\right). \tag{10.3}$$

Here ω is the cyclic frequency of the classical periodic motion in a well at the energy E_0, $p = \sqrt{2m(E_0 - U(x))}$ is the imaginary subbarrier momentum of the particle of mass m, and a is the turning point corresponding to the energy E_0. Using the functions $\psi_1(x)$ and $\psi_2(x)$, we can construct in a two-level approximation the WPs $\psi^I(x) = \psi_0(x)$ and $\psi^{II}(x) = \psi_0(-x)$ localized at the initial time in wells I and II respectively,

$$\psi^I(x) = \frac{1}{\sqrt{2}}\left[\psi_1(x) + \psi_2(x)\right],$$

$$\psi^{II}(x) = \frac{1}{\sqrt{2}}\left[\psi_1(x) - \psi_2(x)\right]. \tag{10.4}$$

Each of the WPs tunnels from well to well with period T equal to

$$T = \frac{2\pi\hbar}{\Delta E}. \tag{10.5}$$

Tunneling from well to well, without changing the shape (coherent tunneling), is a feature of the symmetric potential. In the case of an arbitrary potential, the form of WP changes in the tunneling process: the WP form is sensitive to the details of the form of the potential barrier.

10.2 Dynamical Tunneling

Now we generalize the problem of one-dimensional tunneling discussed above to the case of higher dimensions. The degree of complexity of classical dynamics in multiple dimensions is qualitatively greater than that in one dimension. This fact is clearly manifested in the tunneling effect. This not only applies to the analysis of the usual problem of penetration through the barrier but also leads to the emergence of entirely new tunneling scenarios that have no analogues in one dimension. The features of multidimensional tunneling that interest us can be demonstrated on systems with one and a half and two degrees of freedom, and we restrict ourselves to them.

The simplest example of the fundamentally multidimensional effect associated with tunneling is dynamical tunneling [3]. The concept of dynamical tunneling occurs in systems whose phase space contains domains, the transition between which is prohibited at the level of classical mechanics, but the prohibition is not caused by the potential barrier. Of course, this effect is possible only in systems with more than one degree of freedom, where in addition to the energy, the integrals of motion are sources of the corresponding prohibitions. The new type of tunneling is more complex than traditional (potential barrier) tunneling. The complication is due to the fact that a simple consideration of the potential surface does not detect the prohibition conditions. Instead of static potential surfaces, we have to consider the behavior (dynamics) of the trajectories. Let us return to the above semiclassical solution of the problem of a one-dimensional symmetric double well in order to understand the nature of dynamical tunneling. In this case, when we quantize the system, considering each well separately, we obtain a spectrum consisting of the strictly degenerate doublets. Taking into account only the interaction between the wells due to the overlapping of the exponentially small tails of the wave functions, we get the right result: almost degenerate pairs of levels with the known splitting (10.3).

A situation similar to a one-dimensional symmetric double well may exist in multidimensional potential without the energy barrier. Let us examine [3–5] a dynamical system with reflective symmetry of the phase space T. Suppose that there are two unconnected areas in the phase space, A_1 and A_2, each of which is invariant with respect to the classical dynamics, with mapping to each other by the symmetry operations $A_2 = TA_1$. Consider for concreteness the case that the classical motion in $A_{1,2}$ is regular, that is, when these areas represent islands of stability immersed in a chaotic sea. The additional assumption is made that in the classical limit, there is a set of states $\psi(\mathbf{q})$ that are mainly localized in these areas. Using the standard procedure of quantization of integrable systems, we can independently quantize the motion in each of the areas and construct the degenerate wave functions (sometimes called quasimodes) $\psi^{(1)}(\mathbf{q})$ and $\psi^{(2)}(\mathbf{q}) = \psi^{(1)}(T\mathbf{q})$. In taking into account the interaction between the quasimodes, $\psi^{(1,2)}$ should be replaced by their symmetric

and antisymmetric combinations

$$\psi^{(\pm)} = \frac{1}{\sqrt{2}} \left(\psi^{(1)}(\mathbf{q}) \pm \psi^{(2)}(\mathbf{q}) \right). \tag{10.6}$$

The energy degeneracy between these functions is removed by tunneling processes. But in contrast to the one-dimensional case, the invariant tori in $A_{1,2}$ are not necessarily separated by an energy barrier in the configuration space. The transitions $A_1 \leftrightarrow A_2$ may be prohibited at the classical level of preservation of the integrals of motion other than energy. An example of this type of quantum doublet was first demonstrated in [3]. The authors of that work studied the spectrum and wave functions of the Hamiltonian

$$H = \frac{p_x^2 + p_y^2}{2} + V(x, y); \qquad V(x, y) = \frac{1}{2}\omega_x^2 x^2 + \frac{1}{2}\omega_y^2 y^2 + \lambda x^2 y. \tag{10.7}$$

The parameters used for the calculations are $\omega_x = 1.1$, $\omega_y = 1$, and $\lambda = -0.11$. In the spectrum obtained by the diagonalization of the Hamiltonian (10.7) in the basis of the harmonic oscillator, the pair of states $\psi^{(\pm)}(x, y)$ was found, like the ones shown in Fig. 10.2e, f, with abnormally low splitting of $\Delta E = 0.0001$ and with the energy $E = 13.59$. The sum and difference of these functions give the wave functions $\psi^{(1)}$ and $\psi^{(2)}$, which are similar to those shown in Fig. 10.2c, d. These wave functions are mainly concentrated in the vicinity of the classical periodic orbits shown in Fig. 10.2a, b. It is important to note that despite the absence of the potential barrier, the classical trajectories starting in the vicinity of the phase space of one of the periodic orbits never fall into a neighborhood of another. This

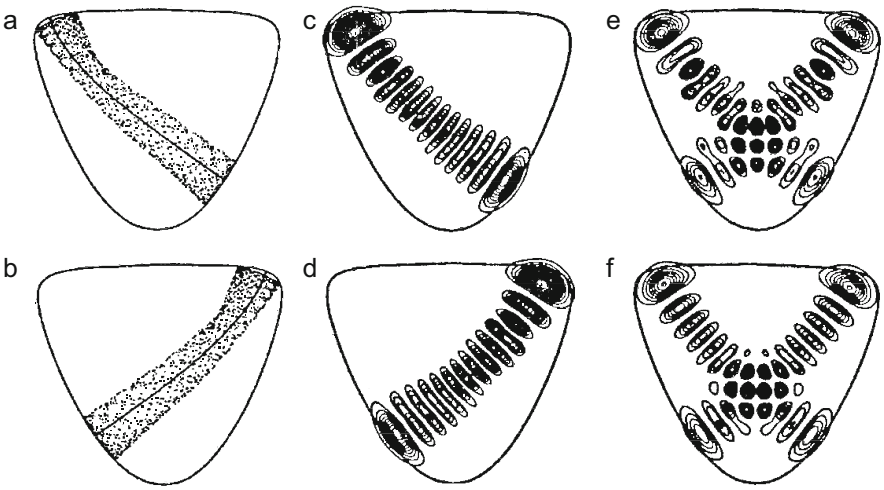

Fig. 10.2 Quantum doublets generated by dynamical tunneling

fact is a consequence of the presence of the additional (other than energy) integral of motion. So the classical trajectories can be "captured" on one or the other side of the dynamical barrier exactly like classical motion in a symmetric double well at energies below the barrier limited by one of the potential wells. The quantum-mechanical situation is fundamentally different. The quasiperiodic orbits, which are similar to the orbits shown in Fig. 10.2a, b with independent quantization, give a pair of degenerate wave functions, as shown in Fig. 10.2c, d. When taking into account the interaction (tunneling), the wave functions $\psi^{(1,2)}$(quasimodes) are not correct eigenfunctions. They should be replaced by the symmetric and antisymmetric combinations $\psi^{(\pm)}$(6) (Fig. 10.2e, f). These pairs are split in frequency by a factor of 10^{-4}, while the fundamental frequency of the oscillations in the potential well is of order unity. The system initially prepared in a state $\psi^{(1)}$ representing the linear combination of the states $\psi^{(\pm)}$, $\psi^{(+)} \pm \psi^{(-)}$, as in the one-dimensional case, may make transitions between this state and the state $\psi^{(2)}$ with a frequency of order $\Delta E/\hbar$. Naturally, the question arises what factors determine the oscillation frequency of the WP, and in particular, if in the phase space of the system there are two symmetric stability islands separated by a chaotic sea, then how this sea affects the (dynamical) tunneling between the islands.

10.3 Dynamical Tunneling: Anharmonic Oscillator with a Periodic Perturbation

A preliminary response to the above question was obtained by Lin and Ballentine [6, 7]. The authors examined a model of a periodically excited double well in which the degree of stochasticity can be adjusted by changing the amplitude of the exciting force. The model Hamiltonian is

$$H = \frac{P^2}{2M} + Bx^4 - Dx^2 + \lambda x \cos \omega_0 t, \qquad (10.8)$$
$$M = 1,\ B = 0.5,\ D = 10.$$

The classical equations of motion are

$$\dot{x} = P/M,$$
$$\dot{p} = -4Bx^3 + 2Dx - \lambda \cos \omega_0 t.$$

To solve the Schrödinger equation, we use the basis $\{|n\rangle\}$ of the harmonic oscillator with the Hamiltonian $\hat{H}$ equal to

$$\hat{H} = \hat{p}^2/2M + \frac{1}{2}M\omega^2 x^2,$$
$$\hat{H}|n\rangle = \left(n + \frac{1}{2}\right)\hbar\omega\,|n\rangle\,. \tag{10.9}$$

The Schrödinger equation in this representation is

$$i\hbar\frac{d}{dt}\langle m|\psi(t)\rangle = \sum_{n=0}^{\infty} H_{mn}\langle n|\psi(t)\rangle. \tag{10.10}$$

To calculate the matrix elements, we have to use the formula

$$\int_{-\infty}^{\infty} e^{-(x-y)^2} H_m(x)H_n(x)dx = 2^n\sqrt{\pi}m!y^{n-m}L_m^{n-m}\left(-2y^2\right), \quad m \le n.$$

Here, H_n are the Hermite polynomials, and L_m^n are Laguerre polynomials. The Schrödinger equation was solved for a given set $\langle n \mid \psi(0)\rangle$ with $0 < n < n_{\max}$. An analysis of the Schrödinger equation (10.10) can be conveniently performed using a transition to the Husimi functions [8] $\rho(x, p)$, defined as

$$\rho(x,p) \equiv (2\pi\hbar)^{-1}\left|\langle\phi_{x,p} \mid \psi(t)\rangle\right|^2, \tag{10.11}$$

where $|\phi_{x,p}\rangle$ is the minimum uncertainty wave packet [9], having average position x and average momentum p, or the coherent state of the harmonic oscillator [10]. In the basis $\{|n\rangle\}$,

$$\langle\phi_{x,p}|n\rangle = \exp\left(-\frac{1}{2}|\alpha|^2\right)\alpha^{*n}/\sqrt{n!},$$

where $\alpha = (x + igp/\hbar)/\sqrt{2g}$, $g = \hbar/M\omega$. The Husimi function provides a quantum analogue of the classical distribution function in the phase space.

We are using as parameters the driving force values $\lambda = 10$ and $\omega_0 = 6.07$. These parameters provide the following structure of the phase space (see Fig. 10.3): two islands of stability are centered at values of $x \simeq -1.5$, $p = 0$ and $x \simeq 4.15$, $p = 0$. We choose as the initial state the WP $|\psi(0)\rangle = |\psi_{x',p'}\rangle$, which is centered in the left island of stability in Fig. 10.3. It can be expected that the WP, which is initially localized in the classically regular area, will remain localized in this area or tunnel slowly therefrom into the chaotic region. Contrary to these expectations, it turned out that there are coherent tunneling oscillations between unrelated regular islands.

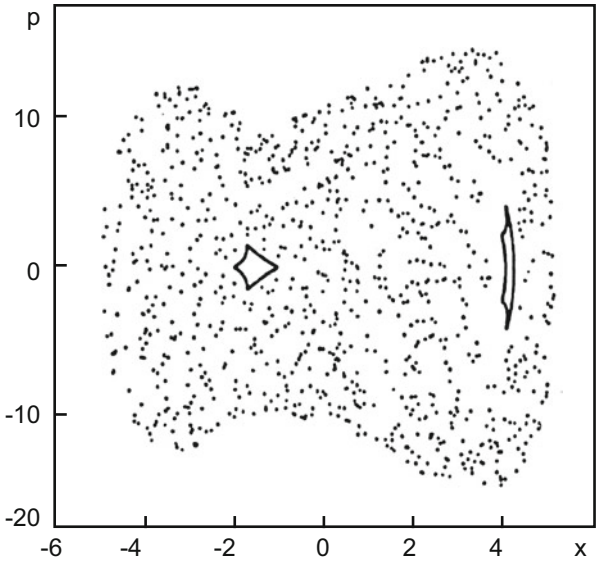

Fig. 10.3 Stroboscopic cross section of the phase trajectories of the Hamiltonian (10.8) [6]

Figure 10.4 shows the time evolution of the Husimi function obtained by numerical integration of the Schrödinger equation in the basis of the harmonic oscillator ($n_{\max} = 115$). Figure 10.4 presents the WP of minimum uncertainty centered in the left island of the stability. With $t = 115\ \tau_0$ ($\tau_0 = 2\pi/\omega_0$), there is a probability close to unity of finding a particle in the next potential well, and in $t = 230\tau_0$, the initial state will be restored with a fairly high degree of accuracy. The characteristic time of tunneling can be identified by a half-period of these oscillations. What is the nature of these tunneling oscillations?

As it turned out [11], the effect can be understood in terms very similar to those we used above in the description of dynamical tunneling. Due to the fact that the considered Hamiltonian is periodically dependent on time,

$$\hat{H}(t) = \hat{H}\,(t + \tau_0)\,,$$

an arbitrary state can be written as a linear combination of the so-called quasienergy states [12]:

$$\psi(x,t) = \sum_{k=1}^{\infty} a_k \psi_k(x,t) = \sum_{k=1}^{\infty} a_k u_k(x,t) e^{-i\varepsilon_k t/\hbar},$$

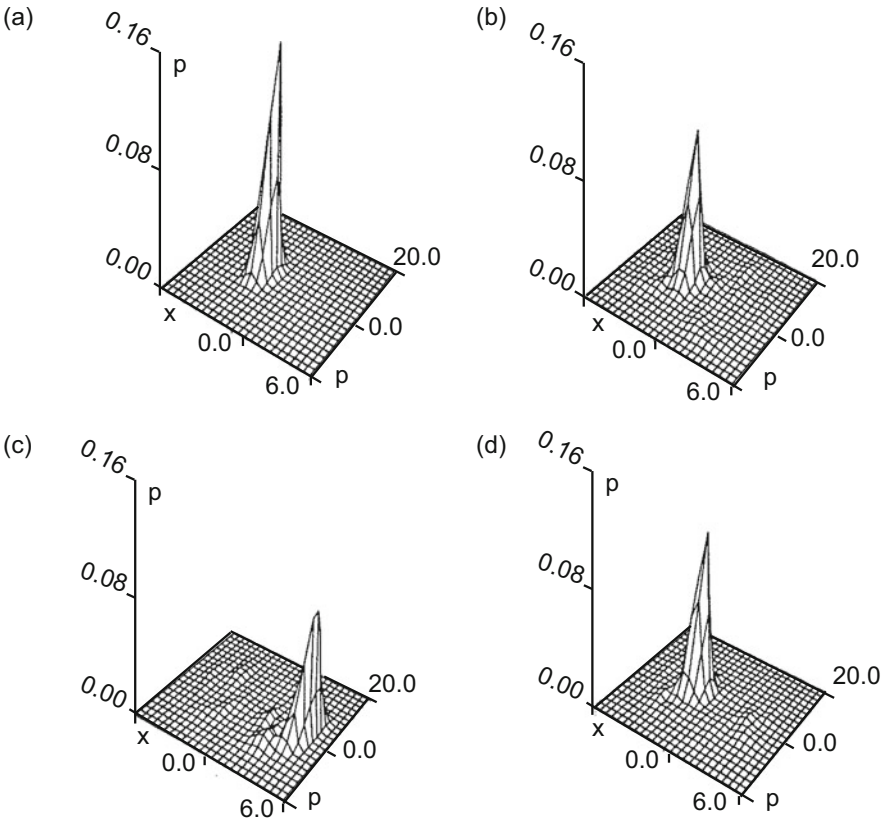

Fig. 10.4 The time-dependence of Husimi functions: (**a**) $t = 0$, (**b**) $t = 5\tau_0$, (**c**) $t = 115\tau_0$, (**d**) $t = 230\tau_0$ [6]

where ε_k is the quasienergy, and the function $u_k(x, t)$ satisfies the equation

$$\left(\hat{H}(t) - i\hbar\frac{\partial}{\partial t}\right) u_k(x, t) = \varepsilon_k u_k(x, t),$$

and furthermore,

$$u_k(x, t) = u_k(x, t + \tau_0).$$

The Hamiltonian (10.8) has a discrete symmetry:

$$H(x, p, t) = H(-x, -p, t + \tau_0/2).$$

This means that the islands of stability in the classical system appear as symmetrically related pairs. For a quantum system, this leads to the fact that the

quasienergy states are even or odd with respect to the replacement $x \to -x$, $t \to t + \tau_0/2$. Consequently the quasienergy states can be grouped in doublets. Each doublet includes even and odd members. If this doublet is localized within a pair of classically regular islands, then it is possible to form from them the WP, which is localized in only one of these islands. This doublet is coherently tunneled (forward and backward) between the regular islands, showing the phenomenon of quantum beating. The tunneling time is inversely proportional to the splitting of the quasienergy in the doublet. The doublets that are localized in such a way are called tunneling doublets. If a tunneling doublet exists, then the WP, initially localized in one of the regular islands, will have coherent tunneling oscillations. But this effect does not occur for doublets that are not localized in the regular islands. Unfortunately, the only way to be sure whether this doublet is localized is to perform a numerical simulation.

10.4 Annular Billiards as a Paradigm for Chaos-Assisted Tunneling

In this section we consider a dynamical system that makes it possible to study qualitatively and quantitatively the relation between the energy splitting that determines the tunneling velocity in the two-level approximation and the structure of the classical phase space [13]. The system is composed of an external circle of radius R ($R = 1$) and an internal circle (disk) of radius $r < R$ (see Fig. 10.5). A point particle moves uniformly in a straight line in the area between the two circles and has elastic mirror reflections on the boundary. In this setting, we are dealing with a two-parameter family of billiards, each of which is defined by a pair of real

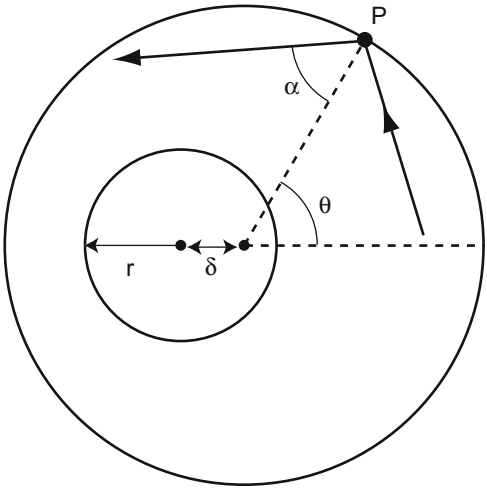

Fig. 10.5 The geometry of a circular billiard

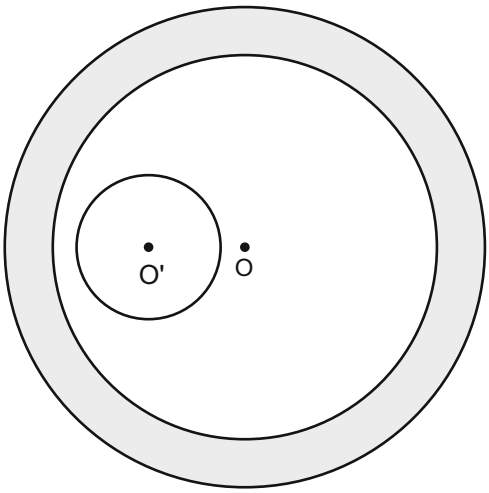

Fig. 10.6 The area (*gray*) of the whispering gallery trajectories

numbers (r, δ), where δ is the eccentricity (shift) of the disk center relative to the center of the external circle.

All the possible trajectories in billiards can be divided into two fundamentally different classes:

1. trajectories that never collide with the internal disk.
2. trajectories that collide at least once with the internal disk.

The trajectories that belong to the first class (and which play a crucial role in further discussion) are commonly called whispering gallery trajectories. They always exist, except in the case of $r + \delta = R$, and are within the shaded symmetric circular area bounded by the external circle and caustic corresponding to the whispering gallery trajectories that are tangent to the internal disk (see Fig. 10.6). For a one-parameter family of billiards $r + \delta = \text{const}$ $(0 < \text{const} < R)$, this area remains the same: if δ varies but $r + \delta$ is kept constant, then all whispering gallery trajectories remain undisturbed.

As the dynamic variables describing the evolution of the system, we can choose the values (see Fig. 10.5) $S = \sin\alpha$, where α is the angle of reflection at the external circle in the point P, and $L = \theta/2\pi R$, where θ is the arc length in P, counted from the intersection point of the line connecting the centers of the circles with the external circle that is closer to the center of the external circle than to the internal one. It is obvious that $|S| \leq 1$ and $|L| \leq 1/2$.

The structure of the phase space in the domain $r + \delta < |S| < 1$ is trivial. A torus in the phase space corresponds to each whispering gallery trajectory in configuration space. The cross section of the torus in the (L, S) plane is a horizontal line $S = \text{const}$; on collision with the external circle, the impact parameter S does not change. Every torus with a given value S can be associated with another torus $-S$, derived from the initial whispering gallery trajectory by changing the rotational direction.

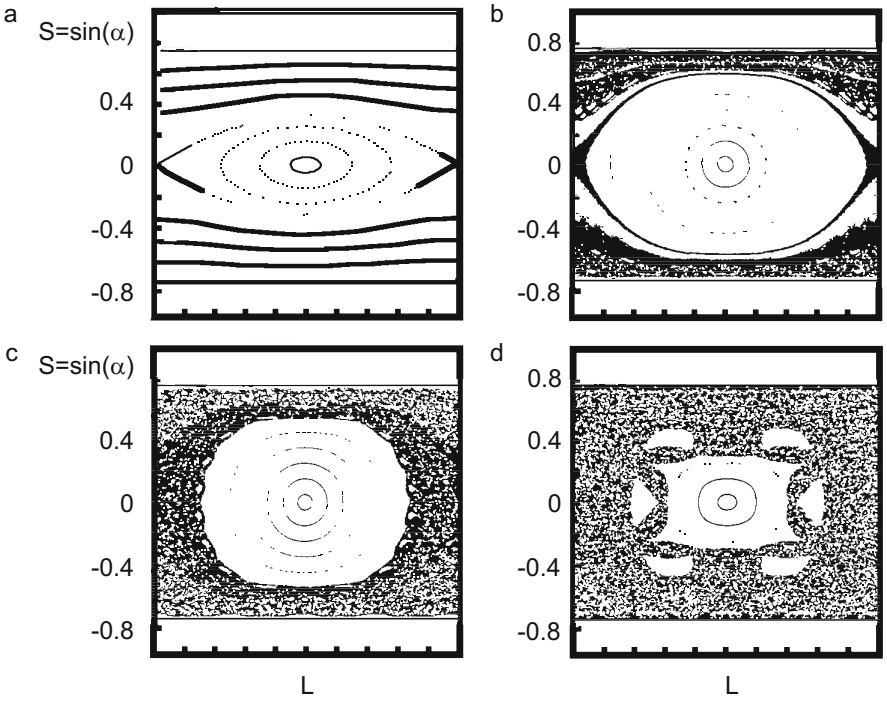

Fig. 10.7 Poincaré sections for $r + \delta = \text{const}$ and different eccentricities δ: (**a**) $\delta = 0.01$, (**b**) $\delta = 0.065$, (**c**) $\delta = 0.10$, (**d**) $\delta = 0.25$ [13]

The rays with a smaller impact parameter $S < r + \delta$ collide with the internal circle, and since the angular momentum in such collisions is not conserved, the motion is no longer integrable (the number of integrals of motion is less than the number of degrees of freedom). This leads to a number of phenomena associated with the concept of a mixed phase space of the nonintegrable system: the islands of stability, immersed in the chaotic sea.

Figure 10.7 shows some Poincaré sections for $r + \delta = 3/4$ and the different eccentricity values δ. For small values of δ (Fig. 10.7a), we can observe around a fixed point at the coordinate origin the presence of libration (or vibration) tori, corresponding to the trajectories that successively collide with internal and external circles. If we reverse this motion, the resulting trajectory will be based on the original torus. Outside the separatrix in the region $|S| \leq r + \delta$, there are rotational tori that like whispering gallery tori, appear in pairs corresponding to the direct and inverse rotation. But in this case (in contrast to the whispering gallery trajectories), the circular motion occurs with the collisions with the internal circle. The rotational tori (unlike the whispering gallery tori) deform when δ is changing, even if $r + \delta = \text{const}$. When δ is increasing (Fig. 10.7b), the region occupied by the libration tori is compressed: part of the vibration tori is destroyed and is replaced by the chaotic

layers. The same holds for part of the rotational tori. In the end, the chaotic sea that appears connects the regions $S = \pm(r + \delta)$ of congruent whispering gallery tori (Fig. 10.7c). When δ is further increased, the region covered by libration tori keeps shrinking (see Fig. 10.7d), until it disappears for $\delta = r$.

The quantum mechanics of annular billiards [5, 13] with boundary conditions of Dirichlet type is described by the Helmholtz equation:

$$(\Delta + k^2)\psi(q) = 0, \tag{10.12}$$

and the requirement that the wave functions vanish at the internal and external boundaries of the billiards. The wave number k is associated with the energy by the relation $E = k^2$. The boundary conditions lead to the quantization of energy (wave number). For the case $\delta = 0$, due to the rotational symmetry, the orbital angular momentum $k \to k_{nm}$ is maintained (as well as the energy), where n is the quantum number of the angular momentum and m is the radial quantum number ($n = 0, 1 \ldots$; $m = 1, 2 \ldots$). Let us recall that the angular momentum quantum number n in the semiclassical limit is associated with the classical impact parameter S by the relation $S = n/k$. The stationary wave function of the circular billiards with $\delta = 0$ is coupled in energetically degenerate doublets, consisting of the components of the angular momentum with n and $-n$. In a system with eccentricity ($\delta \neq 0$), the degeneracy is removed by a violation of rotational invariance. But the doublets are perturbed to different degrees, depending on the relative values of n and $k(r+\delta)$. The symmetry-breaking strongly affects the doublets with a small value of the angular momentum $|n| < k(r + \delta)$, corresponding to the classical motion in which there are collisions with the internal circle. For doublets with small n, the degeneration is removed effectively with the increase of δ. The chaotic eigenstates appear and expand on the states between $-k(r + \delta)$ and $k(r + \delta)$. The higher doublets with the angular momentum $|n| > k(r + \delta)$ change only slightly under the violation of the symmetry (this is understandable, since the trajectories with such impact parameters do not collide with the internal circle, so its movement affects them slightly). The doublets are preserved, and the degeneration is slightly removed. The states are basically symmetric and antisymmetric combinations of n and $-n$ components of the angular momentum:

$$\left|\alpha^{(\pm)}\right\rangle \approx \frac{1}{\sqrt{2}}\left(|n\rangle \pm |-n\rangle\right). \tag{10.13}$$

As explained above, the energy splitting between $\left|\alpha^{(+)}\right\rangle$ and $\left|\alpha^{(-)}\right\rangle$ leads to the tunneling oscillations between the quasimodes $|\pm n\rangle$, linked with whispering gallery tori $\pm S = \pm n/k$ ($S > r + \delta$). A quantum particle prepared in the state $|n\rangle$ will change its rotation from clockwise to counterclockwise and vice versa with the frequency $2\pi\hbar/\Delta E_n$. This tunneling process is a clear example of dynamical tunneling. It occurs in the phase space and not in the configuration space. Whispering gallery tori $\pm S$ are identical in configuration space. Also, in the tunneling process, the overcoming of the potential barrier in the configuration space

does not occur. Indeed, the energy does not play any role in tunneling, because the energy is associated only with the absolute value of the momentum and not with its direction. The tunneling process violates the dynamic law of conservation of angular momentum for the rays with large impact parameters (for small impact parameters it is not conserved because of the internal circle).

We want to find out whether the classical dynamics corresponding to the states $|S| < r + \delta$ (chaotic sea) affect the splitting of quasidoublets, which are constructed on the whispering gallery tori $|S| > r + \delta$. In particular, it is interesting to consider the quasidoublets corresponding to the one-parameter family $r + \delta = \text{const}$. Indeed, when the eccentricity changes, the chaos measure also changes in the intermediate domains (between tori S and $-S$; see Fig. 10.7), but quantized whispering gallery tori remain unperturbed.

We now proceed directly to an analysis of the splitting magnitudes of quasidoublets defining the tunneling speed of wave packets. Why do we expect an increase in this speed? The semiclassical argumentation indicates that the probability distribution associated with the quantized torus decays exponentially outside the torus. A small overlap in the classically forbidden domain of the decaying distributions centered on two congruent quantized tori $(n, -n)$ leads to the tunneling splitting. If there is no chaotic domain between the tori, this overlap is small. However, if the chaotic area between the tori exists, the wave functions corresponding to the tori link first with the chaotic state. Due to the ergodic nature of the chaotic wave functions (the homogeneous distribution of the probability density), the connection between the two tori seems to be more effective than in the case of a regular intermediate state. Hence we can expect that tunneling will be reinforced by the presence of a chaotic region.

To make this argumentation more convincing, it should be confirmed by numerical calculations. Bohigas et al. [13] investigated numerically the transformation of a set consisting of the five tunneling quasidoublets of a one-parameter family of circular billiards with $r + \delta = 0.75$. The observed general tendency represented a dramatic increase in the splitting of quasidoublets (several orders of magnitude) with the increase of the proportion of chaotic phase space (growth of δ). Such a tendency suggests the idea [13] of calling the observed effect chaos-assisted tunneling (CAT). An important feature of the CAT effect is that splitting of quasidoublets increases with an increase in δ. That is why the following observations are important for understanding the physics of this effect:

1. The dependence of the splitting of the eccentricity δ is determined by two independent characteristics of the quasidoublet: the position in the spectrum and the position in the phase space.
2. Quasidoublets that are higher on the spectrum have less splitting.
3. Quasidoublets that are nearest to a chaotic sea have maximum splitting.

It is important to note that the numerical results show significant fluctuations of splittings as a function of eccentricity. Each of the fluctuations is associated with quasicrossing "outsider" chaotic level and considered regular (tunnel) quasidoublet. Because there is no dynamic partitioning of the chaotic region in an unrelated

symmetric field, as is the case in the regular part of the phase space, we have no reason to expect chaotic doublets. Every chaotic state has a fixed parity. At the quasicrossings, the local domain of the spectrum can be described by a three-level model [4] with the Hamiltonian

$$\hat{H} = \begin{pmatrix} E+\varepsilon & 0 & 0 \\ 0 & E-\varepsilon & v \\ 0 & v & E^c \end{pmatrix}.$$

Here, $E \pm \varepsilon$ are the energies of a regular quasidoublet consisting of the symmetric and antisymmetric combinations of the respective quasimodes. In accordance with this model, the even chaotic state $|C\rangle$ of the energy E^c is associated with the state $|+\rangle$, having energy $E - \varepsilon$ as a constant of the interactions v. In practice, one of the constants v and ε dominates over the other. If ε dominates, then we return to the two-level model that has already been considered. Therefore, we assume that the coupling between the states $|C\rangle$ and $|+\rangle$ is dominant, and we set $\varepsilon = 0$. In this case, the splitting of the quasidoublet ΔE is determined by the shift E_+ due to the interaction v. The diagonalization of $\hat{H}$ leads to

$$\Delta E = \begin{cases} \frac{v^2}{E-E^c} & E - E^c \gg v \\ |v| & E - E^c \ll v \end{cases}$$

Thus when changing δ, we see peaks in the splitting of the quasidoublets of height $|v|$ at the intersection of $E^c(\delta)$ with $E_+(\delta)$.

Let us sum up. Unlike the integrable systems with mixed dynamics with the phase space that contains both regular and chaotic areas, a new mechanism of tunneling is demonstrated. The splitting of the doublets, which defines the tunneling velocity in the mixed systems in the two-level approximation, is usually several orders greater than is the case of similar but integrable systems. In contrast to to the direct process whereby the particle tunnels directly from one state to another, CAT corresponds to the following three-step process:

1. tunneling from the periodic orbit to the nearest point of the chaotic sea;
2. the classical spread in the chaotic domain of phase space to the vicinity of another periodic orbit;
3. tunneling from a chaotic sea to another periodic orbit.

In other words, the process of splitting of doublets owes its existence to the reflection symmetry and is not direct but happens through the compound process of destruction of the wave function, piece by piece, close to one regular domain, the chaotic transport in the neighboring symmetric regular area, and restoration of the initial state. Schematically, this three-step process is shown in Fig. 10.8.

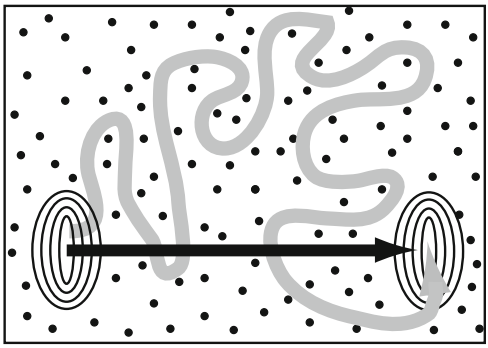

Fig. 10.8 Schematic representation of direct tunneling (*black trajectory*) and the CAT process (*gray trajectory*)

Note that the CAT process is formally of higher order of perturbation theory than direct tunneling. However, the corresponding matrix elements for the CAT are much greater than for direct tunneling. Intuitively, this can be understood as follows: The tunneling from the periodic orbits into a chaotic sea is typically accompanied by significantly smaller violations of classical mechanics than in the case of direct tunneling and therefore has exponentially greater amplitude. More precisely, this means that since a large part of the distance (in a chaotic sea) is a classically allowed transition, we can expect that these indirect trajectories will make a greater contribution to the tunnel flow than direct ones. In the case of direct tunneling, the entire subbarrier trajectory is a forbidden process. The first experimental confirmation of CAT in a microwave version of circular billiards was obtained in [14]. Later, experiments were performed to detect the dynamic tunneling of cold ($10\,\mu$K) cesium atoms in an amplitude-modulated light wave [15]. The arguments in favor of the CAT being responsible for the effect of the transition from superdeformed states of nuclei to states with a normal deformation were given in [16].

Let us briefly consider the experiments using the microwave analogue of annular billiards [14]. This experimental technique makes it possible to work with the spectra in which the size of the splitting of some quasidoublets is several orders of magnitude smaller than the average distance between the levels. Figure 10.9 shows fragments of the spectrum of the circular microwave billiards with superconducting walls in a neighborhood of $f = 9\,$GHz for various values of eccentricity δ [14].

Among a number of the singlet levels, the quasidoublet is clearly visible, and its position in the spectrum changes only slightly with the increase of δ. It becomes possible to measure the quasidoublet splitting of the family of 30 wave functions $(n, m = 1)$. In order to detect the effect of CAT, the quasidoublet splitting should be analyzed as a function of the position of the quasidoublet in the phase space. This can be done using the following considerations. The wave number of states forming a quasidoublet is very close to the concentric case $\delta = 0$. As we pointed out, this happens because the trajectory with a big impact parameter does not collide with the internal circle, so its movement (change δ) weakly perturbs the corresponding

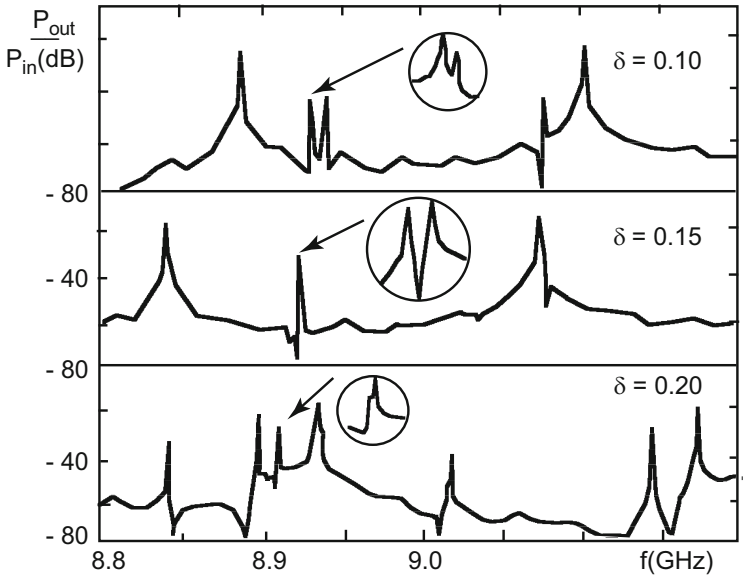

Fig. 10.9 The frequency spectrum of microwave circular billiards with superconductive walls in the vicinity of the frequency $f = 9\,\text{GHz}$ for different parameter values δ. The fragments of the spectrum stretched 50 times by the frequency are shown in *small circles* [14]

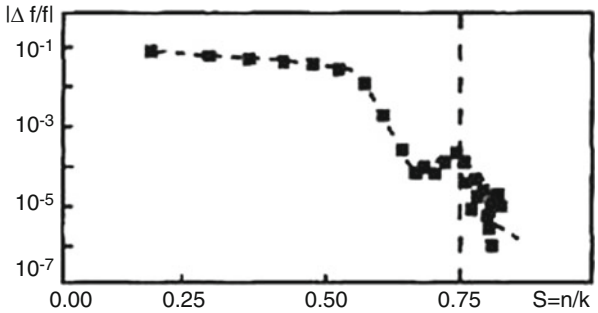

Fig. 10.10 The dependence of the relative doublet splitting $|\Delta f/f|$ on the position of the doublet in the phase space for the value $\delta = 0.20$ [14]

wave functions. This makes it possible to express in terms $S = n/k$ the location of the whispering gallery tori in the phase space. The result of the measurement of the relative doublet splitting $|\Delta f/f|$ for the value $\delta = 0.20$ is given in Fig. 10.10.

In addition to the expected smooth transition from states with big splitting inside the chaotic sea ($S < 0.75$) to states with low splitting in a regular area, the local maximum can be clearly seen in the vicinity of the chaotic sea coast ($S = 0.75$), which can be considered a direct experimental confirmation of the CAT effect.

10.5 Chaotic Nuclear Dynamics

Recent progress in the understanding of chaotic aspects in nonlinear dynamical systems has attracted interest to nuclear dynamics. Indeed, experimental data and modern theory provide a very useful realistic model that allows one to study classical dynamical chaos and the quantum manifestations of classical stochasticity (QMCS).

The chaos concept, despite strong resistance, was introduced in nuclear theory in the 1980s [17–27]. This concept has allowed a fresh look at the peculiarities of nuclear structure [17, 20–23, 28, 29] and nuclear reactions [18, 23, 27], and has helped also to solve a number of old contradictions in nuclear theory [22, 30]. Substantial progress was achieved in the description of concrete nuclear effects [19, 20, 31–33]. Finally, the direct observation of chaotic modes in the simulation of reactions with heavy ions [18] has proven the correctness of the new approach.

Baranger [24] clearly formulated two different approaches to the study of the chaotic aspects of nuclear dynamics.

> Philosophy I. Nuclei are complicated, and chaos comes out of this complication. We expect to find chaos almost everywhere in nuclear physics. Interesting information is in few places without chaos.
> Philosophy II. Chaos is a property of simple systems. The interesting new information may be found in simple areas of nuclear physics that are chaotic.

Currently, Philosophy II finds more and more supporters. Let us illustrate this approach by a few examples.

We address first one of the oldest paradoxes in nuclear theory: the possibility to apply two absolutely opposite physical models—the liquid drop model with strong internucleon interaction and the shell model of no interacting particles—to describe the same object (an atomic nucleus). In order to resolve this paradox in the frame of deterministic chaos (Philosophy II), we use the results of [24, 30]:

1. If the nucleons' motion in the nucleus is regular (integrable dynamics), we could expect the manifestations of strong shell effects, which are well described by the model of independent particles in the potential well.
2. If the nucleons' dynamics are dominated by the chaotic component, then one can expect that the liquid drop model or the Thomas–Fermi approximation would be more adequate.

This hypothesis is based on understanding the mechanism according to which the shell effects are destroyed in the process of the regularity–chaos transition. In the early 1900s, Henri Poincaré pointed out that the main problem of dynamics was to study the perturbations of conditionally periodic motion in a system defined by the Hamiltonian

$$H = H_0(I) + \varepsilon V(I, \theta), \tag{10.14}$$

where $H_0(I)$ is the Hamiltonian of the integrable problem, which depends solely on the action variables I, and $\varepsilon V(I, \theta)$ is the nonintegrable perturbation. The solution of this problem is essentially based on the so-called KAM theorem [34]. This theorem guarantees that the classical integrable system can preserve regular behavior, even at sufficiently strong nonintegrable perturbation. We consider the problem of the shell structure destruction in the quantum spectrum, where the theorem plays the principal role. The residual nucleon–nucleon interaction is a nonintegrable addition to the self-consistent field, obtained for instance in the Hartree–Fock approximation [35]. Therefore we can try to relate the destruction of the shells to the deviation from integrability, or conversely, to relate the growth of the shell effects to the approach of the system to the integrable situation. The possibility for the shell structure to exist at sufficiently strong residual interaction is due to the rigidity of the KAM tori. This mechanism of shell structure evolution seems quite natural, taking into account that the semiclassical quantization procedure [36] is based on similar assumptions.

Let us confirm those general considerations by numerical analysis of the shell structure evolution in the potential of quadrupole oscillations U_{QO} (9.18). As we have seen in Chap. 9, the topology of the potential family $U_{\mathrm{QO}}(x, y; a, b, c)$ is determined by only one parameter $W = b^2/ac$. The region $0 < W < 16$ includes the potentials with a unique extremum—a minimum at the origin, corresponding to a spherically symmetric ground state of the nucleus. We shall restrict our consideration to that area. Recall that for $0 < W < 4$, the motion is regular at every energy, and for $4 < W < 16$, we deal with the R-C-R transition.

Based on these assumptions, let us consider the Hamiltonian of the two-dimensional harmonic oscillator in the role of $H_0 = H\,(b = 0, c = 0)$. The degenerate equidistant spectrum of this Hamiltonian and the eigenstates $|N, L\rangle$ are well known. Evidently, the eigenstates of the exact Hamiltonian $(c, b \neq 0)$ are not already the eigenstates of the operators $\hat{N}$ and $\hat{L}$. Nevertheless, numerical calculations show that one can use the quantum numbers N and L to classify the quantum states, even at sufficiently strong nonlinearity.

The limiting value of the nonlinearity, up to which such a classification is still reasonable (i.e., the shell structure still exists), is related to the quasicrossing of the neighboring levels. By the quasicrossing we understand the approach of the neighboring levels up to a distance of order the numerical accuracy. As one can see from Fig. 10.11a, in the potential with $W = 13$ approaching the critical energy of the transition to chaos determined by the negative curvature criterion (see Chap. 9), the shell structure is destroyed, observed as the emergence of multiple quasicrossings. At the same time, for the potential with $W = 3.9$ (Fig. 10.11b), there is no local instability generated by the negative curvature of the potential energy surface: the motion remains regular at every energy, so the quasicrossings are absent, even for nonlinearity stronger than that in Fig. 10.11a.

The evolution of the shell structure during the R-C-R transition can be followed on the level of wave functions, using the information contained in the coefficients $C^{(k)}_{NLj}$ of decomposition of the wave functions in terms of the harmonic oscillator basis (9.67). For that purpose, similar to the usual thermodynamic entropy, we

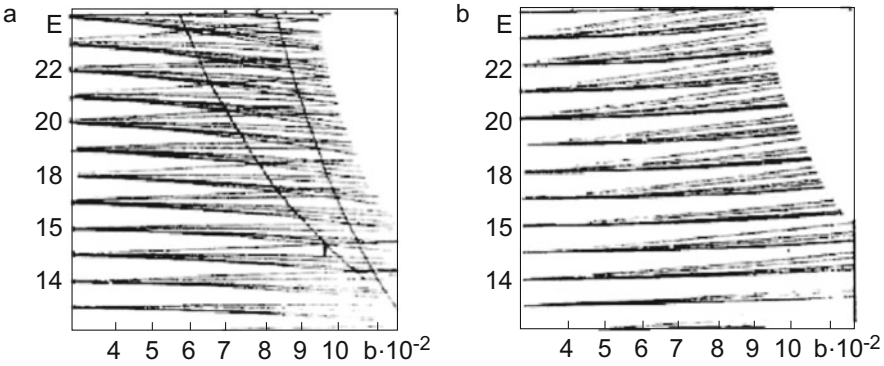

Fig. 10.11 (**a**) Energy spectrum of the quadrupole oscillations Hamiltonian as a function of the parameter b for $W = 13$. The *points* show the quasicrossings. The *solid line* shows the dependence of the critical energy of transition to chaos on the parameter b ($c = 10^{-4}$). The *dashed line* marks the beginning of the quasicrossing region. (**b**) The same for $W = 3.9$. The quasicrossings are absent

introduce [37, 38] the entropy of an arbitrary state k of the exact Hamiltonian H,

$$S(k) = -\sum_{NLj} \left|C_{NLj}^{(k)}\right|^2 \ln \left|C_{NLj}^{(k)}\right|^2 . \tag{10.15}$$

In the regions R_1 and R_2, corresponding to regular motion, the entropy changes correlate with the shell-to-shell transition (see Fig. 10.12). In the chaotic region C, two effects are observed. Firstly, the violation of the quasiperiodic dependence of the entropy on energy reveals the destruction of the shell structure. Secondly, the entropy grows on average monotonically and then reaches a plateau corresponding to the entropy of the random sequence, at energies essentially exceeding the critical energy of the transition to chaos.

The dependence of the shell structure on the type of classical motion is manifest also in such a characteristic of the nucleus as mass. Strutinsky [39] proposed a method to take into account the influence of the shell structure on the nuclear mass. The method is based on the following representation of the total energy of the nucleus as the sum of two terms:

$$U(Z,N,x) = \bar{U}(Z,N,x) + \tilde{U}(Z,N,x), \tag{10.16}$$

where Z and N are the proton and neutron numbers respectively, and x represents a set of the parameters that define the shape of the nucleus. The first term $\bar{U}$ describes the bulk properties of the nucleus, and contains all the contributions that vary smoothly with proton and neutron numbers. The second term $\tilde{U}$ describes the shell effects, related to the shape-dependent microscopic fluctuations. As we have seen

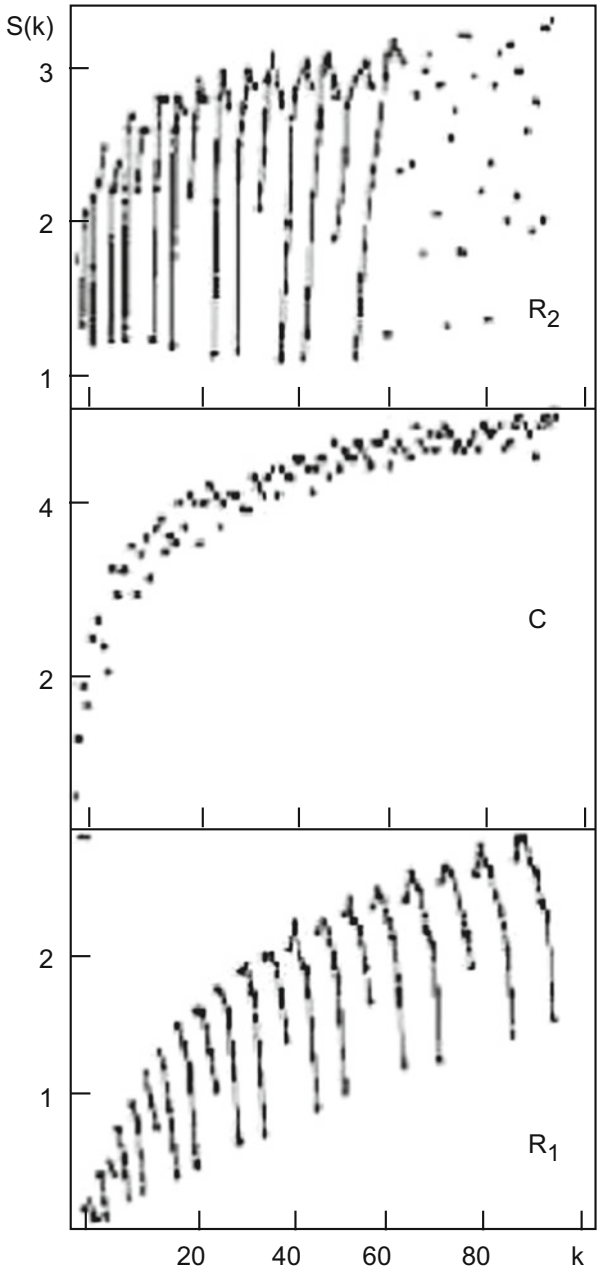

Fig. 10.12 Entropy S_k as a function of state number k for the $U_{\mathrm{QO}}(x, y, W = 13)$ potential. The *solid lines* connecting the points correspond to the shell classification according to N

above, the evolution of the shell structure essentially depends on the type of classical motion. Bohigas and Leboeuf [40] proposed to split the shell correction $\tilde{U}$ into two parts, $\tilde{U} = \tilde{U}_{\rm reg} + \tilde{U}_{\rm ch}$. The two contributions $\tilde{U}_{\rm reg}$ and $\tilde{U}_{\rm ch}$ correspond respectively to the regular and chaotic components of the nucleon motion. According to [40], the presently calculated masses can correctly reproduce only $\tilde{U}_{\rm reg}$; however, the final result for the fluctuations produced by the chaotic part of the motion is in fact of a much more general validity, and may be interpreted as arising from the residual interactions. This approach, as was mentioned above, is equivalent to interpretation of the residual nucleon–nucleon interaction as a nonintegrable addition to the self-consistent field.

From a semiclassical point of view, the Gutzwiller trace formula (see Sect. 9.2) allows one to interpret the shell effects as modulations in the single-particle spectrum produced by the periodic orbits of the corresponding classical dynamics. The trace formula (9.13) allows us to calculate the oscillatory part $\tilde{\rho}(E,x)$ of the total level density $\rho(E,x) = \bar{\rho}(E,x) + \tilde{\rho}(E,x)$. The shell correction to the nuclear mass is computed by inserting the oscillatory part of the density of states into the expression for the energy:

$$\tilde{U}\,(x,A,T) = \int dEE\tilde{\rho}(E,x)f\,(E,T)\,, \tag{10.17}$$

where $f\,(E,T)$ is the Fermi function. In a semiclassical expansion, the leading-order term in the integral comes from the energy dependence of the action. Having set $T = 0$, one obtains

$$\tilde{U}(x,A) = 2\hbar^2 \sum_p \sum_{k=1}^{\infty} \frac{A_{p,k}}{k^2 T_p^2} \cos\left[k\left(I_p - \frac{\pi}{2}\mu_p\right)\right]. \tag{10.18}$$

According to (10.18), the presence of the fluctuations in the total energy is therefore a very general phenomenon that occurs for an arbitrary Hamiltonian, irrespective of the nature of the corresponding classical dynamics. However, their importance (i.e., their amplitude) strongly depends on the properties of the dynamics, particularly on its chaotic or regular type [41, 42].

Let us give one more example to show how the atomic nucleus can be a useful tool for QMCS investigations. One of the alternative approaches [43] to describing quantum chaos is based on the traditional method of time series analysis. Let us consider the energy spectrum as a discrete signal, and a sequence of N energy levels as a time series. We shall characterize the spectra fluctuations by the statistical characteristic δ_n defined as

$$\delta_n = \sum_{i=1}^{n} (s_i - \langle s \rangle) = \sum_{i=1}^{n} w_i, \tag{10.19}$$

where the index n runs from 1 to $N-1$. The quantities w_i characterize the fluctuation of the ith spacing between the nearest neighbors with respect to its average value $\langle s \rangle = 1$. The energy spectrum is assumed to be already unfolded in the standard way, i.e., the initial spectrum was mapped to an auxiliary one ($E_i \to \varepsilon_i$) with unit average value of the level density. Then $s_i = \varepsilon_{i+1} - \varepsilon_i$, $i = 1 \ldots N-1$.

Let us consider how the spectral characteristic δ_n changes during the transition from regular systems to chaotic ones. For that purpose, we calculate the power spectrum $S(k)$ for the discrete series defined as

$$S(k) = \left| \hat{\delta}_k \right|^2, \tag{10.20}$$

where δ_k is the Fourier transform of δ_n,

$$\hat{\delta}_k = \frac{1}{\sqrt{N}} \sum_n \delta_n \exp\left(-\frac{2\pi i k n}{N} \right), \tag{10.21}$$

and N is the time series length.

As an object for detailed investigation of the spectrum, Relano et al. [43] chose the atomic nucleus at high excitation energy, where the density level is very high. They obtained the energy spectrum by diagonalization of the nuclear Hamiltonian with a realistic interaction that reproduces the experimental data quite well. Diagonalization was performed for the different values of angular momentum J, parity π, and isospin T. Among the obtained spectra, they selected a series of 256 consecutive levels with equal J^π, T from the regions of high-level density. In order to reduce statistical errors and to clarify the general trend, the obtained power spectrum $S(k)$ was averaged over 25 level series.

Figure 10.13 represents the results of the averaged power spectrum for the stable Mg^{24} nucleus (the spectrum was obtained by diagonalization of a 2000×2000 matrix) and unstable Na^{34} nucleus (5000×5000 matrix). One can see clearly that the power density of the quantity δ_n is close to a power law, presumably following a simple functional form:

$$\langle S(k) \rangle \sim \frac{1}{k^\alpha}. \tag{10.22}$$

Least-squares fitting gives the results $\alpha = 1.11 \pm 0.03$ for Na^{34} and $\alpha = 1.06 \pm 0.05$ for Mg^{24}. A natural question arises: can there be some universal relations between the peculiarities of the quantum spectrum corresponding to the type of classical motion and the power spectrum of the δ_n fluctuations?

Perhaps the simplest way to answer that question is to compare the power density for the spectrum corresponding to the Poisson statistics to that of the random matrices ensemble, generating the Wigner distribution. The answer obtained in [43] was quite amazing. Ignoring the very high frequency region, where some deviations

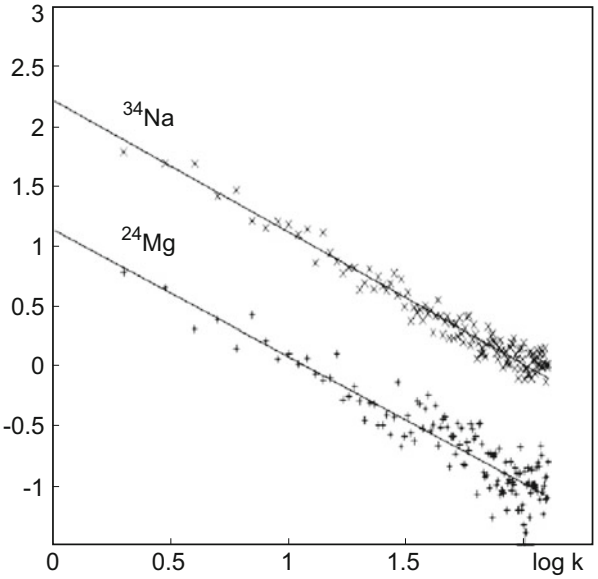

Fig. 10.13 Average power spectrum of the δ_n-function for Mg^{24} from the high-level density region. The plots are displaced to avoid overlapping [43]

were observed probably due to the finiteness of the considered matrices, it was found that $\alpha \simeq 1.99$ for the Poisson spectrum with uncertainty of order of 2 %. In contrast, $\alpha \simeq 1.08$ was found for the Gaussian orthogonal ensemble of the high-dimension matrices, which is usually considered a paradigm of a chaotic quantum spectrum. Therefore, generalizing the obtained results, one can conclude the following [43]: the power spectrum $\langle S(k) \rangle$ behaves as $1/k^{\alpha}$ both for regular and chaotic energy spectra, but the level correlation decreases from the maximum value of $\alpha = 2$ for the regular uncorrelated spectrum to the minimum value of $\alpha = 1$ for chaotic quantum systems.

More generally, this result can be formulated as a hypothesis: the energy spectra are characterized by $1/f$-noise. Recall that the $1/f$-noise (i.e., the flicker-noise) was discovered in the 1920s as a universal satellite of all irreversible stationary processes: its contribution cancels out when the irreversible flows disappear and the system reaches thermodynamic equilibrium.

The proposed hypothesis [43] has a number of attractive features. The considered property characterizes immediately the chaotic spectrum without any reference to properties of other systems (i.e., random matrix ensembles). It is universal for all types of chaotic systems, regardless of whether they are invariant with respect to time reversal, or whether their spin is integer or half-integer. Besides that, the $1/f$ characteristic brings together the quantum chaotic systems with a very wide set of systems from very different branches of science. The flicker-noise is omnipresent.

Therefore, the energy spectra of chaotic systems demonstrate the same type of fluctuations as many others. However, there are no reasons to believe that the $1/f$-noise in the spectral fluctuations of quantum systems implies $1/f$-noise in their classical analogues.

The common conception of the possible stochastization mechanism in quadrupole nuclear oscillations of high amplitude is confirmed by direct observations of chaotic regimes in numerical simulations of reactions with heavy ions [18].

The time-dependent Hartree–Fock theory [35] constitutes a well-defined starting point for the study of such processes. The time-dependent Hartree–Fock equations can be obtained from the variation of the many-body action S,

$$S = \int_{t_1}^{t_2} dt \left\langle \Psi(t) \left| i\frac{\partial}{\partial t} - H(t) \right| \Psi(t) \right\rangle . \tag{10.23}$$

In this expression, H is the many-body Hamiltonian, and the A-nucleon wave function $\Psi(t)$ is chosen to be of determinant form, constructed from time-dependent single-particle states $\psi_\lambda(\mathbf{r}, t)$

$$\Psi(\mathbf{r}_1, \mathbf{r}_2 \ldots \mathbf{r}_A; t) = \frac{1}{\sqrt{A!}} \det |\psi_\lambda(\mathbf{r}, t)| . \tag{10.24}$$

The variation of Eq. (10.23) with respect to the single-particle states ψ_λ and ψ_λ^* yields the equations of motion

$$i\frac{\partial}{\partial t}\psi_\lambda(\mathbf{r}, t) = \frac{\delta \langle H \rangle}{\delta \psi_\lambda^*(\mathbf{r}, t)} \equiv h(\mathbf{r}, t)\, \psi_\lambda(\mathbf{r}, t) , \tag{10.25}$$

and a similar equation for $\psi_\lambda^*(\mathbf{r}, t)$.

The classical nature of these equations can be put into better perspective via the definition of the classical field coordinates $\phi_\lambda(\mathbf{r}, t)$, and conjugate moments $\pi_\lambda(\mathbf{r}, t)$,

$$\begin{aligned} \varphi_\lambda &= \left(\psi_\lambda + \psi_\lambda^*\right)/\sqrt{2}, \\ \pi_\lambda &= \left(\psi_\lambda - \psi_\lambda^*\right)/\sqrt{2}. \end{aligned} \tag{10.26}$$

Then the result is Hamilton's equations:

$$\begin{aligned} \frac{\partial \varphi_\lambda(\mathbf{r}, t)}{\partial t} &= \frac{\delta \langle H \rangle}{\delta \pi_\lambda(\mathbf{r}, t)}, \\ \frac{\partial \pi_\lambda(\mathbf{r}, t)}{\partial t} &= -\frac{\delta \langle H \rangle}{\delta \varphi_\lambda(\mathbf{r}, t)}. \end{aligned} \tag{10.27}$$

The time-dependent Hartree–Fock equation (10.25) and its complex conjugate are solved on a three-dimensional space-time lattice with special initial wave functions [44]:

$$\begin{aligned}\varphi_\lambda(\mathbf{r},t) &\to \sqrt{2}\cos(\mathbf{k}_\lambda\mathbf{r}-\varepsilon_\lambda t)\,\chi_\lambda(\mathbf{r}),\\ \pi_\lambda(\mathbf{r},t) &\to \sqrt{2}\sin(\mathbf{k}_\lambda\mathbf{r}-\varepsilon_\lambda t)\,\chi_\lambda(\mathbf{r}),\end{aligned} \tag{10.28}$$

where ε_λ is the solution of the static Hartree–Fock equations $h\chi_\lambda(\mathbf{r}) = \varepsilon_\lambda\chi_\lambda(\mathbf{r})$, $\lambda = 1\cdots A$, and k_λ is the parameter of the initial boost.

The time-dependent Hartree–Fock calculations for head-on collisions of $He^4 + C^{14}$, $C^{12} + C^{12}\left(0^+\right)$ and $He^4 + Ne^{20}$ were performed by Umar et al. [18] at bombarding energies near the Coulomb barrier. The results are interpreted in terms of their classical behavior. The initial energy and the separation of the centers of the ions are the parameters labeling the initial state. After initial contact, the compound nuclear system (O^{18} or Mg^{24}) relaxes into a configuration undergoing quasiperiodic or chaotic motion. The analysis of nuclear density multipole moments $\left\{M_{LI}(t), \dot{M}_{LI}(t)\right\}$ has been applied for classifying those solutions using Poincaré sections. The definitions of the moments are as follows:

$$\begin{aligned}M_{LI}(t) &= \int d^3 r r^L Y_{LM}(\hat{r})\,\rho_I(\mathbf{r},t),\\ M_{LI}(\omega) &= \int dt \exp(-i\omega t)\,M_{LI}(t),\end{aligned} \tag{10.29}$$

where the isoscalar ($I = 0$) and isovector ($I = 1$) densities are

$$\rho_I(\mathbf{r},t) = \begin{cases}\rho_p(\mathbf{r},t) + \rho_n(\mathbf{r},t) & (I=0),\\ \rho_p(\mathbf{r},t) - \rho_n(\mathbf{r},t) & (I=1).\end{cases} \tag{10.30}$$

The proton ρ_p and neutron ρ_n densities in terms of the field coordinates ϕ_λ and moments π_λ are

$$\rho_q(\mathbf{r},t) = \frac{1}{2}\sum_\lambda\left[\left|\pi_{\lambda,q}(\mathbf{r},t)\right|^2 + \left|\varphi_{\lambda,q}(\mathbf{r},t)\right|^2\right], \quad q = p,n. \tag{10.31}$$

The isoscalar quadrupole mode ($L = 2$, $I = 0$), shown in Fig. 10.14 for the Mg^{24} nuclear system, seems to fill most of the available phase space in the Poincaré section $\left\{M_{LI}(t), \dot{M}_{LI}(t)\right\}$.

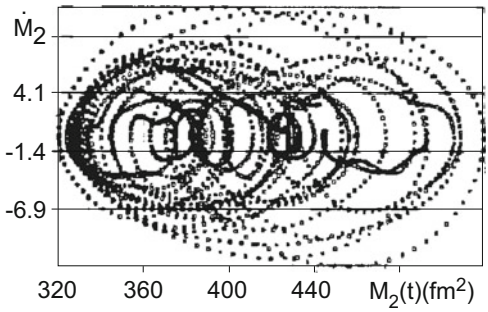

Fig. 10.14 Poincaré section $\{M_{LI}(t), \dot{M}_{LI}(t)\}$ for isoscalar quadrupole mode for the Mg^{24} system [18]

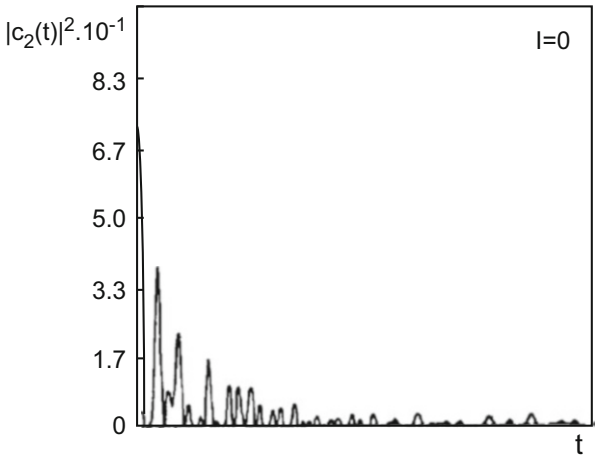

Fig. 10.15 The autocorrelation function $C_{20}(t)$ as a function of time for the isoscalar quadrupole mode in the Mg^{24} system [18]

The corresponding autocorrelation function (Fig. 10.15)

$$C_{20}(t) = \int_{-\infty}^{+\infty} \frac{d\omega}{2\pi} \exp(i\omega t) \, |M_{20}(\omega)|^2 \tag{10.32}$$

damps rapidly. All this favors the view that the corresponding motion is closer to stochastic, rather than quasiperiodic.

In conclusion, let us describe briefly one more nuclear effect, which demonstrates that the nucleus is a laboratory for research of general physical effects such as tunneling, chaos, and phase transitions. Recently, it became clear [45, 46] that superdeformed nuclei offer a new way of understanding nuclear structure. On the one hand, nuclei provide interesting data for the study of these general phenomena; on the other hand, we obtain new information about the nuclear structure.

A superdeformed nucleus is a nucleus that is very far from spherical, forming an ellipsoid with axes in ratios of approximately 2:1:1. Only some nuclei can exist

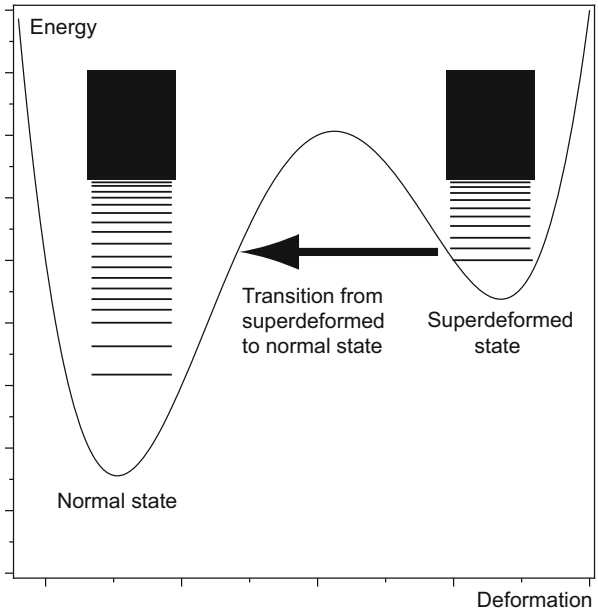

Fig. 10.16 Decay from superdeformed state to normal state

in superdeformed states. These superdeformed nuclei are produced in reactions with heavy ions. Initially accelerated heavy ions, in colliding with nuclei of the target material, produce highly excited and rapidly rotating compound nuclei. These nuclei release part of the excitation energy by the emission of light particles (neutrons, protons, alpha particles) and photons. In all observations of rapidly rotating superdeformed nuclei, rotation breaks off (already at low momentum) when the nucleus suddenly changes its shape and decays to the state that corresponds to lower deformations. Three stages of the transition from the superdeformed state to the normal deformed one are presented in Fig. 10.16 [47]: feeding of superdeformed bands, ordered rotation, and decay from superdeformed to the normal state.

The lowest states in a superdeformed local minimum correspond to high excitations in the main minimum. As a result, the lowest superdeformed states (cold states) are characterized by good quantum numbers and symmetries, while their decays to the main minimum are controlled by the strict rules of selection. In contrast, the normal deformed states at the same energy could correspond to chaotic motion in the semiclassical limit. Statistical analysis confirms this idea: the energy spectrum in this energy region of the main minimum demonstrates all the signs of chaos [47]. This means that in the considered region of nuclei excitation for which the deformation potential allows the existence of the second minimum, a mixed state occurs (see Sect. 9.3). The question is whether the chaos-assisted tunneling mechanism can be used for the description of the transition from the

superdeformed state to the normal deformed one. We should stress that we can consider dynamical tunneling because the transition takes place in multidimensional space: the nuclear shape is characterized by at least two parameters. Aberg [16] estimated in perturbation theory the tunneling probability in two limiting cases. The first limit was the case of no mixing between the normal deformed states (completely regular normal deformed system), while the second was that the tunneling strength is spread out over all normal deformed states (i.e., quantum chaos). For the ratio of the probability of tunneling T^{chaotic} and T^{regular}, Aberg found [16]

$$\frac{T^{\text{chaotic}}}{T^{\text{regular}}} \sim 10^4\text{–}10^6. \tag{10.33}$$

Therefore, we expect the tunneling probability to be enhanced by a factor of 10^4–10^6 if the normal deformed states are chaotic. In other words, the tunneling process connected to the decay out of superdeformed states is strongly enhanced by the chaotic properties of the normal deformed states.

References

1. Razavy, M., Pimpale, A.: Phys. Rep. **168** 305–370 (1988)
2. Landau, L.D., Lifshitz, E.M.: Quantum Mechanics. Pergamon Press, London (1982)
3. Davis, M.J, Heller, E.J.: J. Chem. Phys. **72**, 246–254 (1981)
4. Bohigas, O., Tomsovic, S., Ulmo, D.: Phys. Rep. **223**, 43–133 (1993)
5. Doron, E., Frischat, S.: Phys. Rev. **E57**, 1421–1443 (1998)
6. Lin, W.A., Ballentine, L.E.: Phys. Rev. Lett. **65**, 2927–2930 (1990)
7. Lin, W.A., Ballentine, L.E.: Phys. Rev. **A45**, 3637–3645 (1992)
8. Husimi, K.: Proc. Phys. Math. Soc. Jpn. **22**, 264–314 (1946)
9. Schiff, L.: Quantum Mechanics. McGraw-Hill, New York (1955)
10. Glauber, R.: Phys. Rev. **131**, 2766–2788 (1963)
11. Peres, A.: Phys. Rev. Lett. **67**, 2931–2934 (1991)
12. Zel'dovich, Ya.B.: Sov. Phys. JETP **24**, 1006–1008 (1967)
13. Bohigas, O., Boose, D., de Carvalho, R., Marvulle, V.: Nucl. Phys. A **560**, 197–210 (1993)
14. Dembowski, C., et al.: Phys. Rev. Lett. **84**, 867–870 (2000)
15. Steck, D., Oskay, W., Raizen, M.: Science **293**, 274–278 (2001)
16. Aberg, S.: Phys. Rev. Lett. **82**, 299–302 (1999)
17. Williams, R.D., Koonin, S.E.: Nucl. Phys. A **391**, 72–92 (1982)
18. Umar, A.S., Staer, M.R., Gusson, R.Y., Reinhard, P.-G., Bromley, D.A.: Phys. Rev. C **32**, 172–183 (1985)
19. Bolotin, Yu.L., Krivoshei, I.V.: Yad. Fiz. **42**, 53–56 (1985)
20. Arvieu, R., Brut, F., Carbonell, J.: Phys. Rev. A **35**, 2389–2408 (1987)
21. Bolotin, Yu.L., Gonchar, V.Yu., Inopin, E.V., Levenko, V.V., Tarasov, V.N., Chekanov, N.A.: Fiz. Elem. Chastits At. Yadra **20**, 878–929 (1989)
22. Swiateski, W.: Nucl. Phys. A **488**, 375–394 (1989)
23. Bohigas, O., Weidenmuller, H.: Ann. Rev. Nucl. Part. Sci. **38**, 421–453 (1988)
24. Baranger, M.: Order, Chaos and Atomic Nucleus, preprint (1989)
25. Rotter, I.: Rep. Prog. Phys. **54**, 635–682 (1991)
26. Alhassid, Y., Whelan, N.: Phys. Rev. C **43**, 2637–2647 (1991)
27. Zelevinsky, V.G.: Nucl. Phys. A **570**, 411–421 (1994)

28. Rotter, I.: Fiz. Elem. Chastits At. Yadra **19**, 274–303 (1988)
29. Bolotin, Yu.L., Gonchar, V.Yu., Tarasov, V.N., Chekanov, N.A.: Yad. Fiz. **52**, 669–678 (1990)
30. Bjornholm, S.: Nucl. Phys. A **447**, 117–144 (1985)
31. Blumel, R., Smilansky, U.: Phys. Rev. Lett. **60**, 477–480 (1988)
32. Manfredi, V.R., Salasnich, L.: Int. J. Mod. Phys. E **4**, 625–636 (1995)
33. Manfredi, V.R., Rosa-Clot, M., Salasnich, L., Taddei, S.: Int. J. Mod. Phys. E **5**, 521–530 (1996)
34. Arnol'd, V.I.: Mathematical Methods of Classical Mechanics. Springer, New York (1989)
35. Barts, B.I., Bolotin, Yu.L., Inopin, E.V., Gonchar, V.Yu.: The Hartree-Fock Method in Nuclear Theory. Naukova Dumka, Kiev (1982)
36. Keller, J., Rubinov, S.: Ann. Phys. **9**, 24–75 (1960)
37. Yonezava, F.: J. Non-Cryst. Solids **35**, 29–40 (1980)
38. Reichl, L.E.: Europhys. Lett. **6**, 669–675 (1988)
39. Strutinsky, V.M.: Nucl. Phys. A **95**, 420–442 (1967)
40. Bohigas, O., Leboeuf, P.: Phys. Rev. Lett. **88**, 092502 (2002)
41. Leboeuf, P., Monastra, A.G.: Ann. Phys. **297**, 127–156 (2002)
42. Brack, M., Bhaduri, R.K.: Semiclassical Physics. Addison-Wesley, Massachusetts (1997)
43. Relaño, A., Gómez, J., Molina, R.A., Retamosa, J., Faleiro, E.: Phys. Rev. Lett. **89**, 244102 (2002)
44. Davies, K.T.R., Koonin, S.E.: Phys. Rev. C **23**, 2042–2061 (1981)
45. Aberg, S., Flocard, H., Nazarewicz, W.: Annu. Rev. Nucl. Part. Sci. **40**, 439–528 (1990)
46. Baktash, C., Haas, B., Nazarewicz, W.: Annu. Rev. Nucl. Part. Sci. **45**, 485–541 (1995)
47. Aberg, S.: Z. Phys. A **358**, 269–272 (1997)